



1 **Using large-scale tracer-aided models to constrain ecohydrological partitioning in**
2 **complex, heavily managed lowland catchments**

3

4 Hanwu Zheng^{1,2*}, Doerthe Tetzlaff^{1,2,3}, Christian Birkel⁴, Songjun Wu¹, Tobias Sauter², Chris Soulsby^{3,1}

5

6 ¹Leibniz-Institute of Freshwater Ecology and Inland Fisheries, Berlin, Germany

7 ²Geography Institute and IRI THESys, Humboldt University of Berlin, Berlin, Germany

8 ³Northern Rivers Institute, School of Geosciences, University of Aberdeen, Aberdeen, UK

9 ⁴Department of Geography, University of Costa Rica, San Jose, Costa Rica

10 *Corresponding author: hanwu.zheng@igb-berlin.de

11

12 **Abstract**

13 Tracer-aided modelling (TAM) enhances ecohydrological process understanding, as stable
14 water isotopes ($\delta^{18}\text{O}$ and $\delta^2\text{H}$) can help constrain equifinality and provide complementary
15 information beyond streamflow. Despite being primarily applied in rural (<100km²)
16 catchments with minimal disturbance, TAM may assess epistemic uncertainties from
17 unrecorded human activities affecting streamflow, improving model reliability. This study
18 investigated four sub-catchments (Berste, Wudritz, Vetschauer, and Dobra) in the heavily-
19 managed Middle Spree River basin (ca. 2800 km²), in NE Germany, a strategically vital water
20 resource supplying drinking water to Berlin, Germany's capital, and sustaining agricultural and
21 industrial demands. Detailed evaluation of ecohydrological water partitioning in this
22 evapotranspiration (ET)-dominated region is complicated by heterogeneous land use, extensive
23 hydraulic infrastructure and overall intensive management. We used the spatially distributed
24 tracer-aided model STARR to simulate the effects of natural water storage-flux dynamics and
25 management interventions on streamflow over a 6-year period. Seasonal isotope data used for
26 calibration additionally to streamflow effectively captured subsurface runoff, with isotope



fractionation intensity strongly linked to ET apportionment. This multi-criteria calibration helped reduce equifinality in complex systems with human-induced epistemic challenges. Epistemic errors were manifested as strong trade-offs between the information content of the different calibration constraints (i.e., streamflow and isotopes). Although compromised solutions occasionally failed to meet acceptable performance thresholds for both calibrated variables, such conflicts highlight potentially important mismatches in process representation. Our modelling framework shows the potential for informative insights from wider use of (even sparse) isotope data sets in tracer-aided modelling of complex, heavily managed catchments.

35

36

Highlights:

1. Seasonal isotopes disentangle runoff generation processes.
2. Ignoring minor evaporation in modelling biases ET partitioning.
3. Streamflow & isotope do not constrain spatial ET distribution.
4. Streamflow-isotope trade-offs indicate epistemic errors in observations.
5. Catchments without historical mining effects exhibit large groundwater discharge.

44

45



46 **1. Introduction**

47 Characterizing ecohydrological processes in sparsely monitored catchments with
48 heterogeneous landscapes is inherently challenging due to spatially variable flow pathways and
49 non-stationarity in climate inputs (Hrachowitz et al., 2013; McDonnell et al., 2007). This
50 challenge can be even greater in catchments heavily modified by human activities, where a
51 long and on-going history of disturbance can fundamentally alter processes and functioning
52 (Marx et al., 2021). Distributed hydrological models are useful tools in addressing these
53 challenges and are capable of capturing the dominant processes across spatio-temporal scales
54 through regional parameterization (Fatichi et al., 2016). However, increasing model
55 complexity to capture catchment heterogeneity makes it difficult to identify when models give
56 “the right answer for the wrong reason” (Kirchner, 2006). In most catchments, rainfall and
57 streamflow are the only available data for modelling. Streamflow-based calibration has
58 therefore been the standard approach in hydrological modelling, leveraging the widespread
59 availability of river discharge data to estimate model parameters across diverse catchments
60 (Hrachowitz et al., 2013). However, calibration based on streamflow observations (single or
61 multiple gauges) alone are usually insufficient to constrain hydrological model uncertainty, as
62 certain parameters remain non-identifiable (Herrera et al., 2022). Consequently, simulations
63 with multiple parameter sets can give equally plausible outputs, with equifinality being a
64 pervasive issue in model applications (Beven, 2006). Multi-criteria calibration, that is,
65 leveraging complementary datasets (e.g., soil moisture, ET, groundwater) in addition to
66 streamflow, to mitigate this effect is increasingly common (Kuppel et al., 2018; Oliveira et al.,
67 2021; Shah et al., 2021; Wu et al., 2023).

68

69 Stable water isotopes ($\delta^{18}\text{O}$, $\delta^2\text{H}$) are a potential solution that can help identify water sources,
70 flow paths, and transit times, thus revealing process heterogeneity in catchments (Klaus and



71 McDonnell, 2013; Sprenger et al., 2015). They are often used as complementary datasets to
72 streamflow, offering additional insights into catchment hydrological behavior that can aid
73 parametrization and modelling (Fenicia et al., 2008). In many cases, the integration of isotopes
74 into models has advanced process representation, improving understandings of water
75 partitioning and storage-flux interactions in heterogeneous landscapes (Birkel and Soulsby,
76 2015; Luo et al., 2024; McDonnell and Beven, 2014; Smith et al., 2022). Consequently, tracer-
77 aided models (TAMs) have been increasingly applied worldwide (Jung et al., 2025). However,
78 many TAM studies showed inevitable trade-offs in model performance resulting from
79 conflicting information in the streamflow and isotopes data (Birkel et al., 2015; Scudeler et al.,
80 2016; Wu et al., 2023). Such differences can highlight errors in model structure and
81 inappropriate process conceptualization (Beven, 2006; McDonnell et al., 2007; Wu et al., 2025).
82 This is sometimes inevitable, such as when unknown anthropogenic influences affect
83 hydrological behaviour. For example, unregulated water abstractions and artificial drainage
84 can alter streamflow patterns, but simulations may still reproduce observed discharge, even
85 without parameterising human effects into models via overfitting, which can result in a
86 misleading representation of the system. In addition, using some observations as “soft data”
87 (i.e. qualitative information or measured data that are not used in calibration) to constrain
88 models can alleviate some of the above issues (Efstratiadis et al., 2010; Wu et al., 2023).
89 However, failing to rigorously evaluate trade-offs between isotopes and streamflow risks
90 producing structurally biased results, even if models achieve seemingly acceptable objective
91 metrics for both datasets. Explorations of how these trade-offs in multi-criteria modelling using
92 isotopes to help better understand hydrological processes and indicating further improve
93 models are relatively rare.

94



95 Most TAMs focus on rural catchments (Soulsby et al., 2015) with limited anthropogenic
96 disturbance (Yang et al., 2023), while complexities of ecohydrological processes are
97 exacerbated in human-dominated systems where management measures can fundamentally
98 alter hydrological connectivity and function (Wada et al., 2017). This creates critical unknowns
99 in characterizing hydrological processes under anthropogenic alterations. In this regard,
100 advancing tracer-aided methods to systematically evaluate hydrological dynamics at different
101 spatial and temporal scales in heavily managed catchments can have advantages in modelling
102 (Smith et al., 2021).

103

104 In this study, water stable isotopes ($\delta^{18}\text{O}$ and $\delta^2\text{H}$) were used in a tracer-aided hydrological
105 model (Spatially distributed Tracer-Aided Rainfall-Runoff, STARR), to help constrain
106 estimates of ecohydrological partitioning and water balance compartments in four heavily
107 modified sub-catchments of the Middle Spree catchment (MSC) in eastern Germany. These
108 include the effects of agricultural irrigation, land use change, urbanisation and historic lignite
109 mining with associated groundwater pumping. The area impacts a major national water
110 resource as the Spree river forms Berlin's water supply and ongoing pressures and intensifying
111 climate change have the potential to threaten future water provision and ecosystem stability
112 (Arndt and Heiland, 2024). Despite this significance, quantitative evaluation of
113 ecohydrological processes in the MSC is currently limited, as records of intensive water use
114 are not always available, historic impacts are often undocumented and parameterising these
115 human influences in hydrological models are difficult. Therefore, this study aims to provide a
116 preliminary insight of ecohydrological couplings between storage and fluxes as well as effects
117 on the partitioning into runoff generation processes and ET fluxes in parts of the MSC, with
118 the following specific objectives addressed:

119 1. Assessing trade-offs between streamflow and isotope-aided constraints in calibration of



- 120 ecohydrological modelling in intensively managed lowland catchments.
- 121 2. Quantifying the spatio-temporal dynamics of the water balance in intensively managed
- 122 lowland catchments during wet and dry periods.
- 123 3. Examining how management activities can bias ecohydrological models and advancing
- 124 isotope-aided methods to disentangle process dynamics in human-dominated systems.



125 **2 Materials and Methods**

126 **2.1 Study catchment**

127 The Mid-Spree catchment (MSC) is located in the SE of Brandenburg, Germany (Figure 1).

128 The 2806 km² sub-basin forms the middle part of the much larger Spree catchment (10105
129 km²), accounting for 28.6% of the entire catchment area. Within the MSC, the Spree River
130 flows from Cottbus to Beeskow and through the Spreewald UNESCO Biosphere Reserve,
131 which is an extensive wetland area. Climate is sub-continental with low precipitation and hot
132 and dry summers (Pusch et al., 2009). Mean annual precipitation in the headwaters of the entire
133 Spree catchment range from 600mm to 1000mm, decreasing to 556 mm in the MSC, making
134 it one of the driest regions in Germany. Average monthly temperatures range between 19.3°C
135 in summer (June to August) and 1.9°C in winter (December to February), respectively. Annual
136 potential evapotranspiration, based on the FAO-56 Penman-Monteith equation (Deutscher
137 Wetterdienst (DWD), 2024), reaches 726mm, making the MSC water-limited and highly
138 susceptible to climate change.

139

140 The topography is flat and 80% of MSC varies between 42 to 78 m.a.s.l, though the maximum
141 elevation is 155.6 m.a.s.l. The course of Spree River through the MSC has a very low gradient
142 (0.027 %).

143

144 We selected four gauged sub-catchments in the MSC: the river Berste (gauged at Bruckendorf),
145 the Wudritz catchment (gauged at Ragow), the Vetschauer Mill Creek (gauged at Vetschau),
146 and the Dobra catchment (gauged at Boblitz), in the southern tributaries of the Spree River as
147 the main study catchments (Figure 1). They are mostly dominated by croplands (encompassing
148 some of the most extensive areas in the MSC), with pasture and coniferous forests forming the



149 other two major land uses in the four sub-catchments, accounting for 12-20% and 18-30% of
150 the area, respectively.

151

152 The geology of the sub-catchments is dominated by fluvial and meltwater sediments, especially
153 along the river reaches, while artificial fills (from mining spoil) constitute a major part in the
154 Wudlitz and Dobra catchments, as a result of historic lignite extraction (Landesregierung
155 Brandenburg, 2024). Sandy soils (58.7% of the area) and clay- sands (29.7%) dominate these
156 sub-catchments, while peat soils are sporadically distributed.

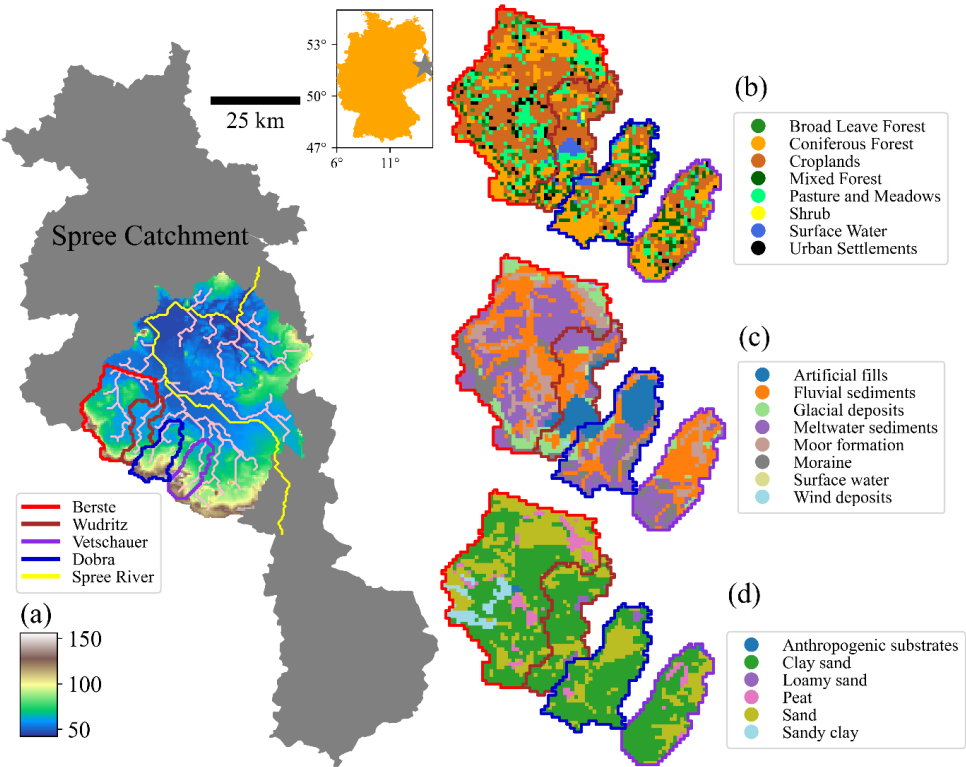
157

158 The four sub-catchments, like much of the MSC, were influenced by intense lignite mining
159 activities between 1960-1990 (Pusch and Hoffmann, 2000). Of our study sites, the Wudritz and
160 Dobra catchments were most severely affected, though lakes and restored areas now occupy
161 the former mining areas. These lakes are relatively small, shallow and linked to streamflow in
162 an unknown and non-stationary way. Pumped mine water (sump water), from de-watering
163 former open-cast mines in the Altdoberm, Schlabendorf and Seese regions was discharged to
164 the southern tributaries of the Spree River. After the sharp decline in lignite production in the
165 early 1990s, discharge volumes from southern tributaries in the MSC to the Spreewald are
166 believed to be close to the pre-mining situation since 2018 (Landesregierung Brandenburg,
167 2024). However, more generally in the Spree catchment, the decline of pumped sump water
168 volumes has been faster than the replenishment of the groundwater deficit, and the lowered
169 groundwater table leads now to a high risk of lower river flows and water shortages in the MSC,
170 and constitutes a threat to Berlin's water supply further downstream (Arndt and Heiland, 2024).
171 At present, in these four sub-catchments, drinking water is extracted from groundwater wells,
172 while authorised water withdrawals in channels for agriculture are limited to spring and
173 summer months (Landesregierung Brandenburg, 2024).



174

175



176

177 *Figure 1. (a) Elevation, river network and catchment borders, (b) land use, (c) geology, and*

178 *(d) soil types of the four sub-catchments in the MSC.*

179



180 *Table 1. Catchment characteristics of the MSC and its sub-catchments (Berste, Wudritz,*

181 *Dobra, Vetschauer)*

Land use (%)	MSC	Berste	Wudritz	Dobra	Vetschauer
Urban settlements	5.5	5.2	3.5	3.0	4.2
Surface water	2.9	0.2	7.7	3.0	0.7
Pasture and meadows	19.2	17.2	12.3	13.7	13.7
Croplands	30.6	48.4	44.9	25.6	33.9
Shrub	0.8	0	0.5	0.4	0.2
Coniferous forest	29.7	20.6	18.5	36.6	30.4
Mixed forest	8.5	6.5	8.1	12.0	14.1
Broad leave forest	2.8	1.9	4.5	5.7	2.8
Geology (%)					
Artificial fills	4.7	1.0	23.7	24.1	0
Fluvial sediments	25.7	27.7	29.9	20.5	49.4
Glacial deposits	9.3	8.2	11.4	3.2	5.6
Meltwater sediments	28.0	35.0	21.0	29.8	23.7
Moor formation	17.3	18.1	5.2	5.7	12.5
Moraine	12.2	9.5	8.6	16.7	8.8
Wind deposits	2.8	0.5	0.5	0	0
Soil (%)					
Peat	8.5	7.3	0	1.5	5.1
Clay sand	29.7	51.4	70.9	71.0	66.6
Sand	58.7	34.1	24.9	26.2	27.4
Clay	0.6	0	0	0	0
Sandy clay	1.1	6.8	0	0	0
Anthropogenic substrates	1.1	0.4	0	0	0.9
Loamy sand	0.3	0	4.2	1.3	0
Area (km²)	2806.3	316	101.3	131.8	107.8

182

183 **2.2 The STARR model and adaptations to simulate low-relief and different land use**

184 The spatially distributed tracer-aided rainfall-runoff (STARR) model (van Huijgevoort et al.,
185 2016) integrates the general conceptual structure of the HBV-light hydrological model
186 (Lindström et al., 1997; Seibert and Vis, 2012) in a distributed, gridded framework that enables
187 flux tracking of water and tracers through catchments. It is operated in the PCRaster Python
188 framework (Karssen et al., 2010). The STARR model includes a module for tracking of
189 stable water isotopes and tracer mixing (van Huijgevoort et al., 2016; Ala-aho et al., 2017). As
190 a fully distributed model, hydrological fluxes are simulated in each grid cell based on a simple
191 reservoir structure and water balance equations (Figure S1). This has been successfully applied
192 in TAMs across a range of catchments at multiple scales (0.2-2500 km²) in contrasting



193 environments (Ala-Aho et al., 2017; Correa et al., 2020). The basic hydrological components
194 and a brief summary of the STARR model are given in the supplementary materials (Appendix
195 A), while van Huijgevoort et al., (2016) and (Dehaspe et al., 2018) provide more detailed
196 descriptions.

197

198 Some of the assumptions of the STARR model, which was originally developed for
199 mountainous catchments subsequently adapted for tropical and cold regions, are not applicable
200 in the lowland catchments studied here (the detailed equations used in modified STARR model
201 are shown in Table S1). The topographical wetness index was not used to separate hillslope
202 and lowland areas for runoff generation as in previous applications. Further, runoff routing was
203 determined by the Manning equation (Chow, 1959), rather than assigning a pre-defined
204 velocity.

205

206 Further, fractionation of stable water isotopes by evaporation in soil and interception storage
207 was adapted to follow the Craig-Gordon model (Craig and Gordon, 1965), rather than being
208 simulated by empirical representations (as in van Huijgevoort et al., 2016, Correa et al., 2020).
209 The partitioning of evapotranspiration (ET) in the original STARR model was not applicable
210 in the MSC as the isotopic composition of evaporation was sometimes more enriched than
211 calculated isotopes of ambient atmospheric vapour (Chakraborty et al., 2018). Therefore, the
212 partitioning method from HYDRUS-1D (Simunek et al., 2013) was used here, where the
213 transpiration originates from, and is linearly related to, soil and groundwater saturation. In
214 order to keep parameter consistency, we adapted the interception module to the one developed
215 in the HYDRUS-1D and the EcoPlot models (Stevenson et al., 2023), with the interception
216 volume and the maximum capacity being controlled by LAI. Channel grid cells were distinct
217 in representing different runoff and routing processes. Roughness (Manning coefficient) used



218 in the kinematic wave equation was defined as 0.025 in the channel grid cells as recommended
219 in Chow (1959), while other non-channel grid cells were assigned the values similar to van der
220 Sande et al., (2003) and according to the land use (Table S2). The channel width used in the
221 kinematic wave equation was estimated from recent Google earth maps (03.08.2024), while
222 the width for non-channel grid cells was defined as the grid cell size (i.e., 500 m). Other
223 parameters were the same for all grids. Explicit parameterization of anthropogenic factors (i.e.,
224 major water withdrawn in Berste, restored lakes in Wudritz and Dobra) was excluded due to
225 insufficient data, and the influences will be evaluated.

226

227 **2.3 Data Acquisition**

228 2.3.1 Forcing Datasets

229 The spatial resolution of the model grid was defined at 500 m as a trade-off between adequate
230 spatial detail and computation time (Smith et al., 2021). All datasets listed in Table 2 were
231 downscaled or upscaled to the same resolution for consistency.

232

233 The meteorological inputs were acquired from twenty weather stations in or near the study
234 catchments (i.e., measuring precipitation (P), temperature (T), relative humidity (RH)) and grid
235 products of potential evapotranspiration (PET) operated by the German Weather Service
236 (DWD) were used, and the station datasets were linearly interpolated to spatially distributed
237 (500 m) inputs. The 8-day composite LAI dataset at 500 m resolution (MCD15A3H V6.1) was
238 used to characterise LAI dynamics. The dataset was accessed through Google Earth Engine
239 (GEE). The cloud masking process was based on GEE and linear resampling at daily resolution
240 was conducted, corresponding to the other input datasets. A global product to estimate the
241 stable water isotopic composition (Interannual Monthly Mean values) of rainfall from (Bowen



242 and Revenaugh, 2003) was used and set as daily rainfall isotope input to the model constant in
243 each month and equal to the monthly product value.

244

245 2.3.2 Datasets for model calibration and evaluation

246 Daily discharge from 2018 to 2023 and seasonal streamwater isotope data were collected
247 during 2021-2023 in the four catchments at the Bruckendorf (Berste), Ragow (Wudritz),
248 Boblitz (Dobra), and Vetschau (Vetschauer mill creek). Gauging stations (Figure 1) were used
249 for model calibration (Table 2). Stable isotopes were sampled every season over three years
250 (2021, 2022, 2023) at the river outlet of the four catchments (for detailed sampling procedure
251 refer to Chen et al. (2023)). Further, MODIS ET (MOD16A2GF from GEE) and PML ET
252 (Zhang et al., 2019) 8-day composite products were compared with simulation results to
253 evaluate evapotranspiration simulation. Despite uncertainties, the PML product aligned better
254 with flux tower (51.8922 N, 14.0337 E) records in the Spreewald (Table 2) indicating its
255 usefulness as a comparator for modelling results (Figure S2).

256

257 *Table 2. Overview of the datasets used in this study*

Forcing datasets	Temporal resolution and period	Spatial resolution
P, T, RH	Daily; Jan 2014 - Dec 2023	20 stations
PET	Daily; Jan 2014 - Dec 2023	1 km × 1 km cells
Discharge	Daily; Jan 2014 - Dec 2023	4 stations
Rainfall isotopes	Monthly; Jan 2014 - Dec 2023	5 × 5 arc minutes
LAI	8 days; Jan 2014 - Dec 2023	500 m × 500 m cells
Calibration datasets		
Discharge	Daily; Jan 2014 - Dec 2023	4 stations
Streamwater isotopes	Seasonally; Jan 2021 - Dec 2023	4 sample locations
Evaluation datasets		
PML ET	8 days; Jan 2014 - Dec 2023	500 m × 500 m cells
MODIS ET	8 days; Jan 2014 - Dec 2023	500 m × 500 m cells
FLUXNET	Daily; Jan 2011 - Dec 2014	1 station in the Spreewald

258

259



260 **2.4 Model parameterisation, sensitivity analysis and calibration**

261 2.4.1 Model parameterisation

262 The number of calibrated model parameters was minimised and therefore some of the
263 parameters were assigned fixed values (Table S2). In total, 35 parameters were included for
264 calibration and the assigned ranges for calibration were mostly adapted from previous
265 applications of the STARR model, with some adjustments appropriate to the characteristics of
266 the study catchments (Table S2). Parameters representing soil characteristics were distributed
267 according to land use types (i.e., urban, water, pasture, cropland, shrub, forest) given the close
268 correlation between land cover and soil type in the region (see (Smith et al., 2021)). The flux
269 processes from interception to soil storage (throughfall and stemflow) are different in forest
270 and non-forest land use, as contrasting canopy characteristics affect the rainfall partitioning
271 (Guevara-Escobar et al., 2007), and the corresponding parameters were determined separately.

272

273 2.4.2 Sensitivity analysis (SA)

274 We employed the Morris Method (Morris, 1991) to identify the sensitive parameters. The
275 calculation used the SAFE tool (Sensitivity Analysis for Everybody, Pianosi et al., 2015). The
276 elementary effects (reflecting the sensitivity of each parameter) were calculated through
277 perturbing the starting parameter by a certain variation based on a radial one-at-a-time strategy.
278 Nash Sutcliffe Efficiency (NSE) (Hodson, 2022) of simulated streamflow or streamwater
279 isotopes, corresponding to calibration scheme, was used as the objective function in calculating
280 the elementary effects (Table 3). The Latin-Hypercube sampling method (Pianosi et al., 2015)
281 was selected to determine the starting parameter and following perturbation. The mean
282 elementary effect of each parameter was used to indicate the sensitivity of the corresponding
283 parameters. Parameters related to pastures, croplands, and forests were more sensitive than



284 others, as they cover majority of the catchment area (Table 4), and the estimated
285 ecohydrological fluxes are mainly shown for these three land uses.

286

287 2.4.3 Model calibration

288 The modified STARR model was run at daily time steps for the period from 2014 to 2023. A
289 4-year spin-up period (2014-2017) was applied, and the remaining six years were used for
290 calibration. The multi-objective non-dominated sorting genetic optimization algorithm II
291 (NSGA-II) (Blank and Deb, 2020; Deb et al., 2002) was applied to derive the Pareto-optimal
292 solutions. Five distinct calibration schemes were conducted based on measurements (i.e.,
293 streamflow and/or stream isotopes) at the outlet of the four catchments and are detailed in Table
294 3. The first scheme (discharge-only based calibration) was calibrated only on the streamflow
295 of all four catchments (multi-gauged streamflow calibration) using the NSE values of simulated
296 streamflow as the objective function. Considering the potential for heterogeneity in the
297 hydrological functioning of each catchment and to assess the additional information content of
298 the isotope data in the modelling, calibrations (the other four schemes as in Table 3) were also
299 carried out in each catchment independently and based on NSE values of simulated streamflow
300 and isotope (isotope-aided calibrations) (Table 3). Simulations based on NSGA-II were
301 conducted with 40 generations and 200 individuals in the population per generation, and the
302 first pareto front in the 40th generation were employed as the solution. No validation period
303 was employed, as the present study attempted to better constrain ecohydrological processes in
304 the MSC, rather than for forecasting applications. Further, calibrating to the full available data
305 and skipping model validation has been found more robust than the traditional split-sample
306 approach in hydrological modelling (Shen et al., 2022).

307



308 *Table 3. Five calibration schemes based on measured streamflow and isotope at the outlet of*
 309 *the four catchments. Sensitivity analysis was conducted separately on isotope and discharge*
 310 *measures in schemes 2-5.*

Calibration scheme	Streamflow	Isotope	Objective function in SA
Scheme 1	Berste		$\sum_i NSE_i$, i includes streamflow in all sub-catchments used in the scheme
	Wudritz		
	Vetschauer		
Scheme 2	Dobra		$NSE_{streamflow}$ or $NSE_{isotope}$
	Berste	Berste	
Scheme 3	Wudritz	Wudritz	$NSE_{streamflow}$ or $NSE_{isotope}$
	Vetschauer	Vetschauer	
Scheme 4	Dobra	Dobra	$NSE_{streamflow}$ or $NSE_{isotope}$
	Berste	Berste	

311



3 Results

3.1 Model performance

3.1.1 Discharge simulations

315

316 *Table 4. The 6 most sensitive parameters in each calibration scheme. Subscript p, c, f represent*

317 *pasture, croplands, forest, respectively. kS , kG LP, INT_{α} , K control processes of runoff from*

318 *soil, runoff from groundwater, Actual ET, interception and ET partitioning, respectively; and*

319 *FC is the soil water storage capacity.*

Scheme1	Scheme2	Scheme3	Scheme4	Scheme5
Discharge	isotope	discharge	isotope	discharge
kS_f	kS_c	kS_c	kS_c	kS_f
kS_c	K	kS_f	kS_f	kS_c
kS_p	LP_c	kS_p	kS_c	kS_p
LP_f	FC_c	LP_c	INT_{α}	LP_f
LP_c	kS_f	FC_c	kG	K
FC_c	kG	INT_{α}	kS_p	INT_{α}

320

321

322

323

324

325

326

327

328

329

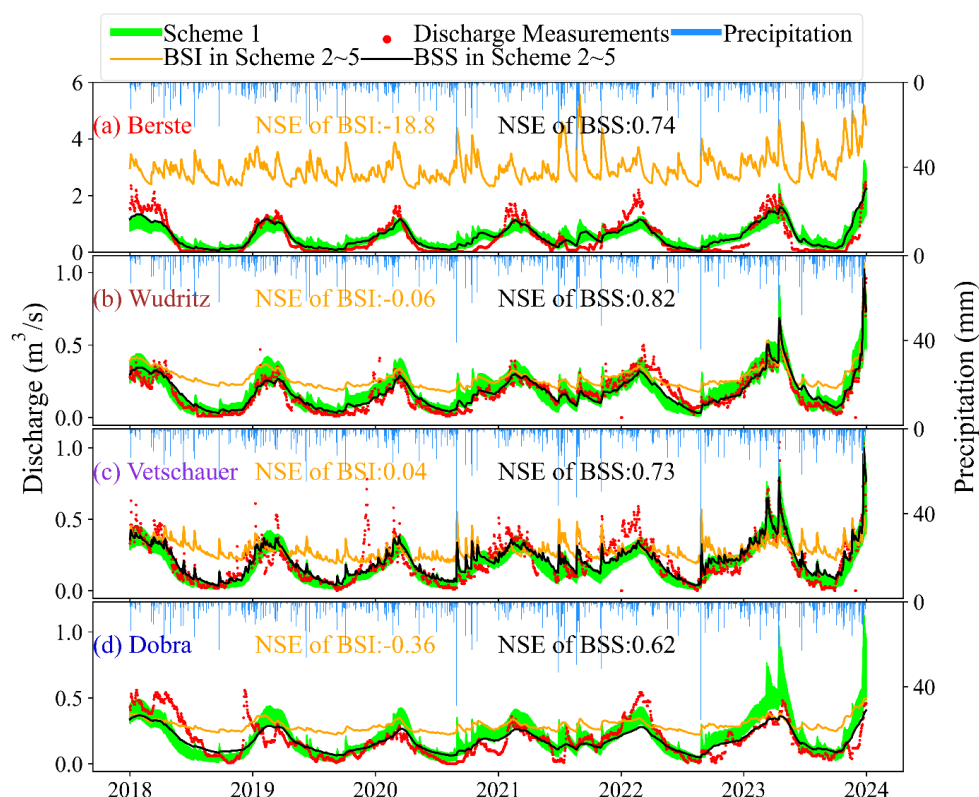


Figure 2. Discharge simulations at the outlet of each catchment based on each calibration scheme. (a) Berste; (b) Wudritz; (c) Vetschauer; (d) Dobra. “BSI” and “BSS” are abbreviations for the simulation with Best Simulated Isotope and Best Simulated Streamflow, respectively.

Discharge-only based calibrations (scheme 1) and parameter sets with the best simulated streamflow (BSS) in isotope-aided calibrations (scheme 2-5) successfully captured discharge dynamics in each catchment with average NSE (Figure 2) mostly >0.6 (Table 5). The uncertainty bands in scheme 1 were relatively large, but bracketed the measurements for most of the time at most sites (Figure 2). The averaged NSE were slightly lower than BSS in schemes 2-5, suggesting the trade-offs in balancing performance across the four individual catchments. However, variations in scheme 1 and BSS (schemes 2-5) generally underestimated peak flows

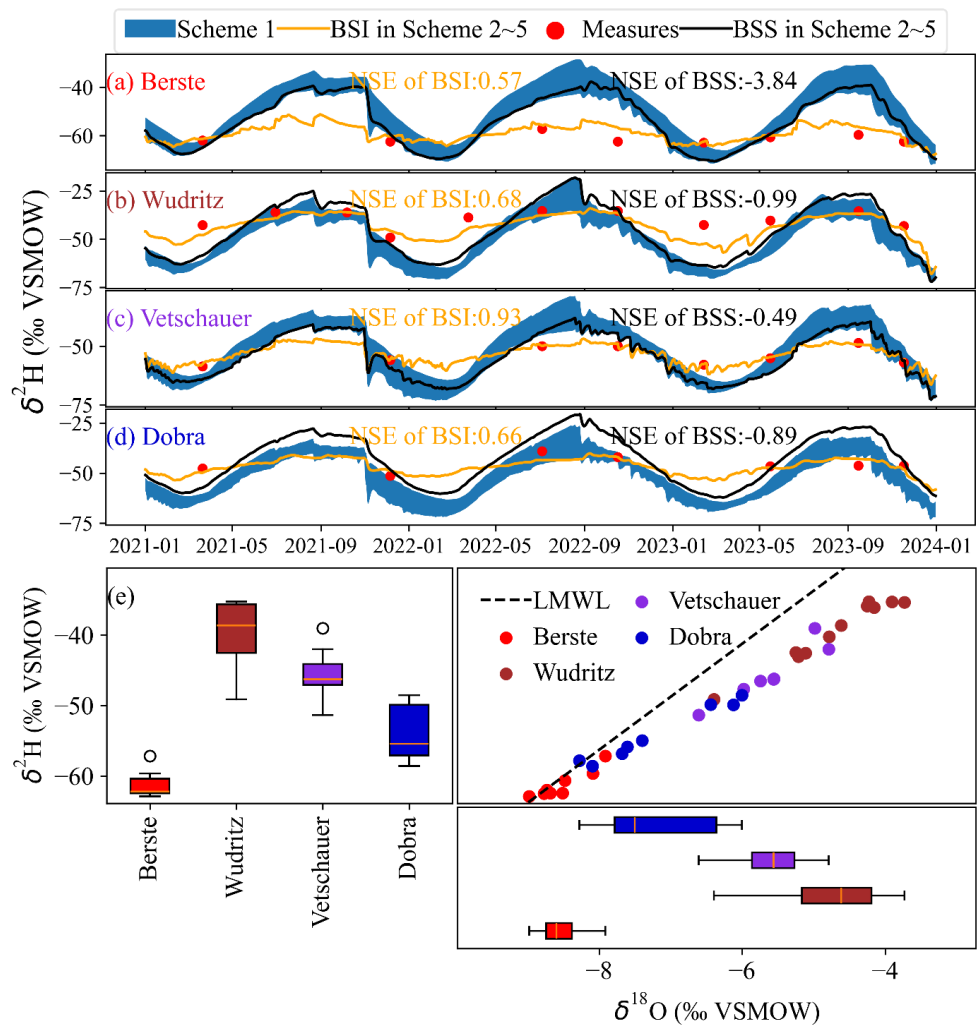


343 and overestimated base flows. Parameter sets with the best simulated isotopes (BSI) in schemes
344 2-5 gave large biases in modelled streamflow compared to measurements, showing much
345 higher base flow, lower variations, and higher frequency of high flows, particularly in Berste
346 and Vetschauer where pronounced overland flow contributions were simulated (see section
347 3.2.2).
348



349 3.1.2 Isotope dynamics

350



351

352 *Figure 3. Isotope simulations at the outlet of each catchment based on each calibration scheme.*

353 *(a) Berste; (b) Wudritz; (c) Vetschauer; (d) Dobra; and (e) Dual isotope plots for streamwater*
354 *isotopes from Jan 2021 to Dec 2023 in each catchment.*

355

356 The stream isotope signatures in the four catchments showed contrasting characteristics.

357 Overall, apart from the Berste, streamwater isotopes in each catchment plotted below the local



358 meteoric water line (LMWL), reflecting fractionation processes. The similar alignment of
359 isotopes along a shared local evaporation line indicates comparable atmospheric moisture
360 demand among the catchments (Figure 3). The Berste exhibited the most depleted isotopic
361 signature ($\delta^2\text{H}$: $\sim -62\text{‰}$), while Wudritz was the most enriched catchment ($\delta^2\text{H}$: $\sim -38\text{‰}$), and
362 their enrichments positively correlated with the extent of surface water area, although all
363 catchments have low surface water coverage ($< 8\%$) (Figure 3). Simulations in scheme 1 and
364 BSS in schemes 2-5 reproduced the seasonal isotope dynamics, with summer enrichment and
365 winter depletion (Figure 3). However, the variability of isotopes was overestimated, although
366 mean simulations and measurements were comparable. This showed that different flow paths,
367 mixing processes and fractionation effects in the catchments were problematic in the discharge-
368 only based calibrations (scheme 1) or BSS in isotope-aided calibrations (schemes 2-5). BSI in
369 schemes 2-5 yielded much more consistent simulations of the isotope dynamics, although this
370 came at the cost of much poorer discharge performance (Figure 3). The low NSE values
371 between simulations and measures are because of the coarse temporal scale of samples and
372 deviations in single sample point could result in large degradation in NSE values (Table 5).

373

374

375

376

377

378

379

380

381

382



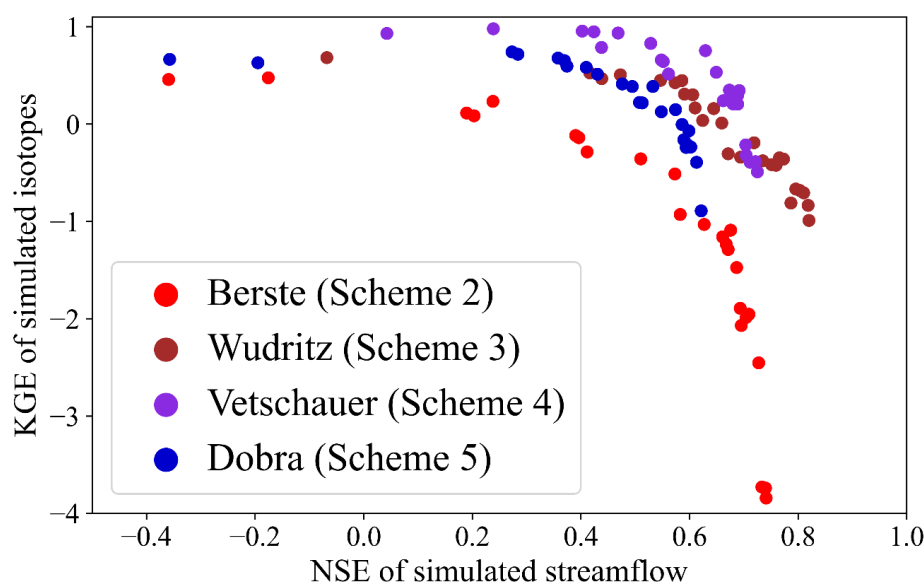
Table 5. NSE and KGE values for discharge and isotopes at different locations based on the different schemes. Values at multiple locations were only calculated in calibration scheme 1, while the metrics of the other four schemes (“schemes 2-5”) were given at corresponded calibrating outlets (i.e., values in Berste, Wudritz, Dobra and Vetschauer are from Schemes 2-5, respectively). The slash “/” separates results in the two ends of the pareto front, namely “BSS/BSI”.

Locations	Scheme 1				Schemes 2-5			
	Discharge		Isotope		Discharge		Isotope	
	NSE	KGE	NSE	KGE	NSE	KGE	NSE	KGE
Catchments								
Berste	0.69	0.57	-55.9	-3.93	0.74/-18.8	0.66/-4.03	-42.0/-1.05	-3.84/0.57
Wudritz	0.77	0.83	-7.85	-0.76	0.82/-0.06	0.85/0.24	-5.18/-0.02	-0.99/0.68
Vetschauer	0.63	0.66	-2.48	-0.77	0.73/0.04	0.75/0.17	-1.44/0.96	-0.49/0.93
Dobra	0.46	0.69	-4.30	-0.56	0.62/-0.36	0.56/0.02	-5.95/0.51	-0.89/0.66

3.2 Trade-offs between streamflow and isotope-based calibrations

3.2.1 Pareto front of simulations

The Pareto front of simulations from schemes 2-5 show the range of potential solutions of streamflow and isotopes. Points in the middle of the Pareto front represent the compromised “trade-off” solutions based on both streamflow and isotopes (Figure 4). Berste resulted in lower NSE or KGE of both isotopes and streamflow than the other three catchments, while the compromised trade-off solutions in Vetschauer were most satisfying, and its Pareto front was the narrowest (Figure 4). The unsatisfactory solutions for Berste reflected the conflicting information provided by isotope and streamflow data under the existing model structure and potentially reflected unknown processes resulting from the intense management.



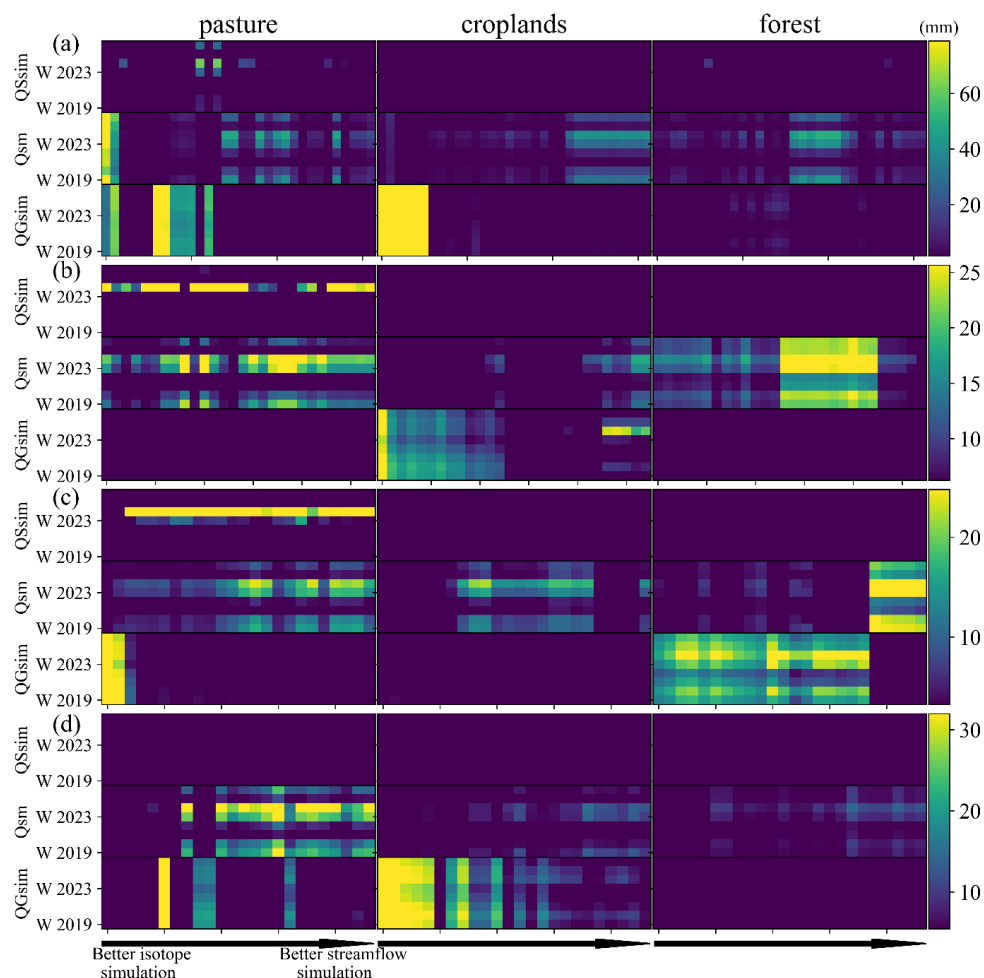
401

402 *Figure 4. Pareto front of simulations in schemes 2-5. Simulations on two ends of the front were*
403 *excluded in this plot. KGE of the compromised solutions in Berste, Wudritz, Vetschauer and*
404 *Dobra can reach 0.14/0.23, 0.54/0.45, 0.62/0.75 and 0.43/0.40 in streamflow/isotope.*

405

406 3.2.2 Impact of calibration on contributing runoff generation processes

407 Runoff generation from soil storage was the most sensitive hydrological processes in the
408 simulations in all calibration schemes (no matter whether isotope measures were considered),
409 while groundwater contributions were highlighted by isotopes in Berste and Vetschauer (Table
410 4). According to the solutions on the Pareto front, runoff was mostly generated from the soil
411 and groundwater storages, while overland flow was limited in the pasture in the winter or spring
412 of the wet year of 2023 in two of the catchments (Figure 5). For the parameter sets that
413 produced the best streamflow simulations, runoff was mainly sourced from the shallower soil
414 stores in all three major land uses, while this contribution gradually decreased in simulations
415 for the opposite end of the Pareto front with groundwater sources being more important for
416 simulations with better isotope performance (Figure 5).



417

418 *Figure 5. Total seasonal runoff from contrasting sources for three land uses for each catchment*
 419 *during 2019 and 2023 (winter, spring, summer, fall of 2019 and 2023 along Y-axis from bottom*
 420 *up, and “W” in the Y-label means winter) in the first Pareto front of (a) Berste (scheme 2); (b)*
 421 *Wudritz (scheme 3); (c) Vetschauer (scheme 4); (d) Dobra (scheme 5). “QGsim” and “Qsm”*
 422 *represent runoff from groundwater and soil water, respectively, while “QSSim” is*
 423 *instantaneous overland flow. Each pixel in the plot is the total seasonal amount of runoff. The*
 424 *X axis from left to right represents results from BSI to BSS.*

425

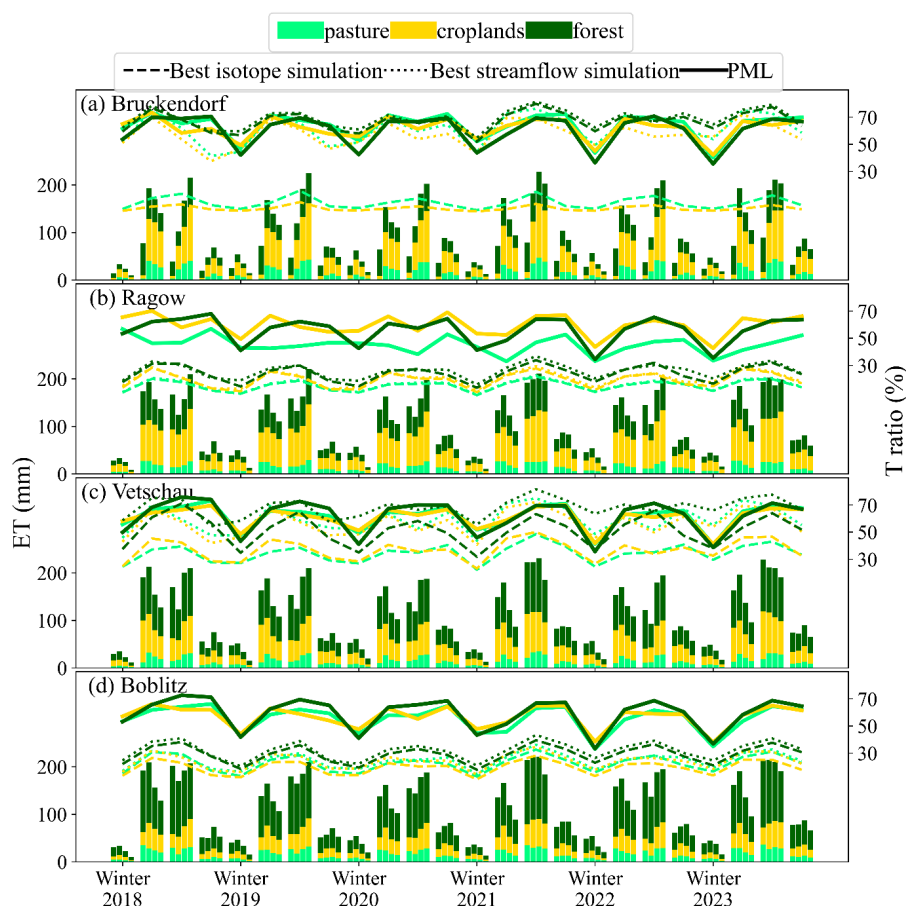


426 Runoff generation from soil and groundwater storages showed seasonality with higher
427 streamflow in winter. This pattern was further intensified during the wet year of 2023 (Figure
428 5). Runoff from soil in parameter sets with better simulated streamflow presented lower
429 influence in croplands of all four catchments. Runoff from groundwater in simulations with
430 better isotope performance was more evident in croplands than the other two land uses, except
431 for the Vetschauer catchment (Figure 5). Subsurface water flowing through capillary flux (from
432 groundwater storage to soil) and soil seepage (soil to groundwater) was consistent along the
433 Pareto front of Wudritz and Dobra, with high contribution of both fluxes in croplands (Figure
434 S3). The stronger influence of subsurface processes in Berste and Vetschauer was only re-
435 produced in simulations with better isotope performance (Figure S3).

436

437 3.2.3 Impact of calibration on ET estimates and ET partitioning

438 The sensitivity of parameters controlling the movement of water to the atmosphere (ET) was
439 important, although they had contrasting order in each calibration scheme. Except for the
440 underestimated ET in parameter sets with better simulated isotopes in Berste, parameter sets
441 along the Pareto front had consistent annual ET volume in each catchment (from 400 to 500
442 mm/year in dry to wet years), and mostly aligned with both satellite estimates. ET showed
443 strong seasonality with peaks in spring and summer in model simulations (Figure 6; Figure S4).
444 This aligned with the satellite ET observations. Simulations at both ends of the Pareto front
445 showed higher springtime ET yet lower modelled ET in summer across all catchments
446 compared to the remote sensed products, except for BSI in Berste. These differences decreased
447 during wet summers (e.g., 2021 and 2023) (Figure 6; Figure S4). BSI (except for Berste) in
448 schemes 2-5 had lower spring ET and higher summer ET compared to BSS. This seasonal shift
449 in BSI aligned better with temporal patterns of remote sensed ET (Figure 6).



450

451 Figure 6. Seasonal total ET and transpiration ratio (T/ET) from simulations (a) Berste in
 452 scheme 2; (b) Wudritz in scheme 3; (c) Vetschauer in scheme 4; (d) Dobra in scheme 5, and
 453 RS products. Bars and lines indicate ET and T ratios, respectively. Each season contains four
 454 bars, ordered from left to right as follows: simulation with best simulated isotope and best
 455 streamflow, MODIS and PML ET products. ET values from each land use were scaled
 456 according to their area proportion, and the stacked bar value approximately represents the
 457 total seasonal ET of the sub-catchment.

458

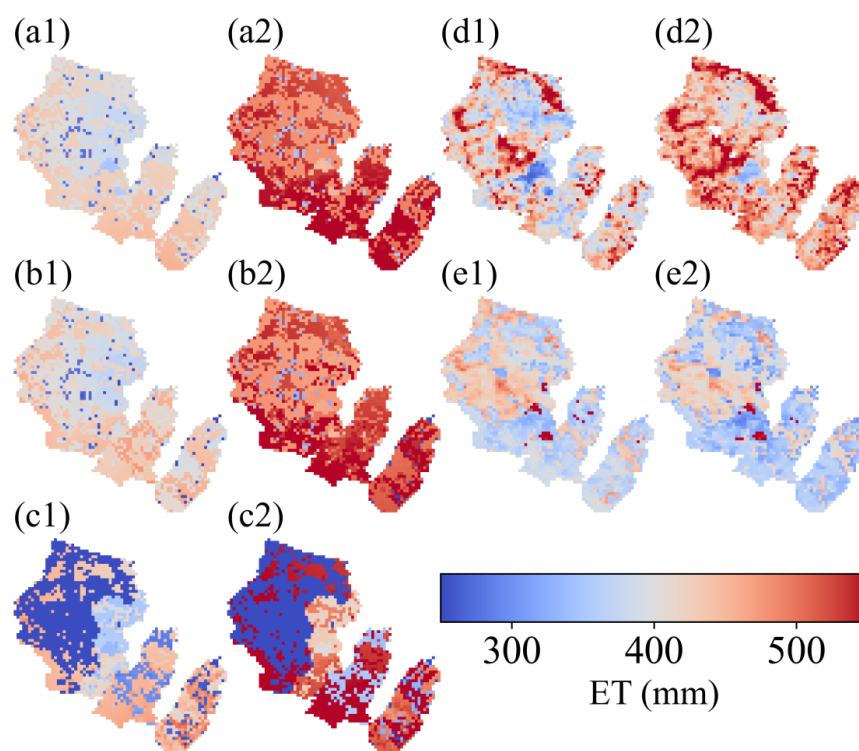


459 Simulations in scheme 1 and BSS (schemes 2-5) exhibited higher consistency with spatial
460 patterns of MODIS ET compared to BSI (schemes 2-5). Additionally, elevated ET was
461 consistently captured along the channel reach in Berste, the upper catchment in Wudritz, and
462 across the whole catchment of Vetschauer and Dobra (Figure 7), although the simulated spatial
463 variability in ET remained less pronounced than the MODIS estimates. However, high ET in
464 the PML product was more consistent with croplands distribution, which indicated the potential
465 irrigation in croplands that has not been conceptualized in the current model structure (Figure
466 7).

467

468 In terms of ET partitioning (into E and T), soil water storage capacity became more sensitive
469 for simulations constrained by isotopes as the corresponding parameters ranked higher
470 compared to discharge-only based simulations. This is consistent with the importance of
471 fractionation in the variation of isotopes (Table 4). In all catchments, the transpiration ratio
472 from each land use had similar temporal dynamics (summer peaks and winter troughs), and
473 was higher in forest than in the other two land uses (Figure 6; Figure S4). In Vetschauer, most
474 simulations of transpiration ratios in the Pareto front in all three land uses aligned with the
475 PML estimates, with 50-70% and 30-40% (dependent on land use; with forest being higher) in
476 summer and winter shown in compromised solutions, respectively, although with slightly
477 lower values in BSI. The consistent and high transpiration along the Pareto front was shown in
478 Berste, and only some of the better simulated isotope simulations in the Pareto front highly
479 underestimated transpiration (Figure 6, Figure S4). In contrast, simulations (schemes 2 and 5)
480 in Wudritz and Dobra showed notably lower transpiration ratios, and only a small part of
481 simulations in the Pareto front reached RS levels (Figure S4).

482



483

484 *Figure 7. Spatial distribution of ET in the four catchments. (a) Scheme 1; (b) BSS in schemes*
485 *2-5; (c) BSI in schemes 2-5; (d) MODIS ET; (e) PML ET. Suffix “1” and “2” means dry year*
486 *of 2019 and wet year of 2023, respectively.*

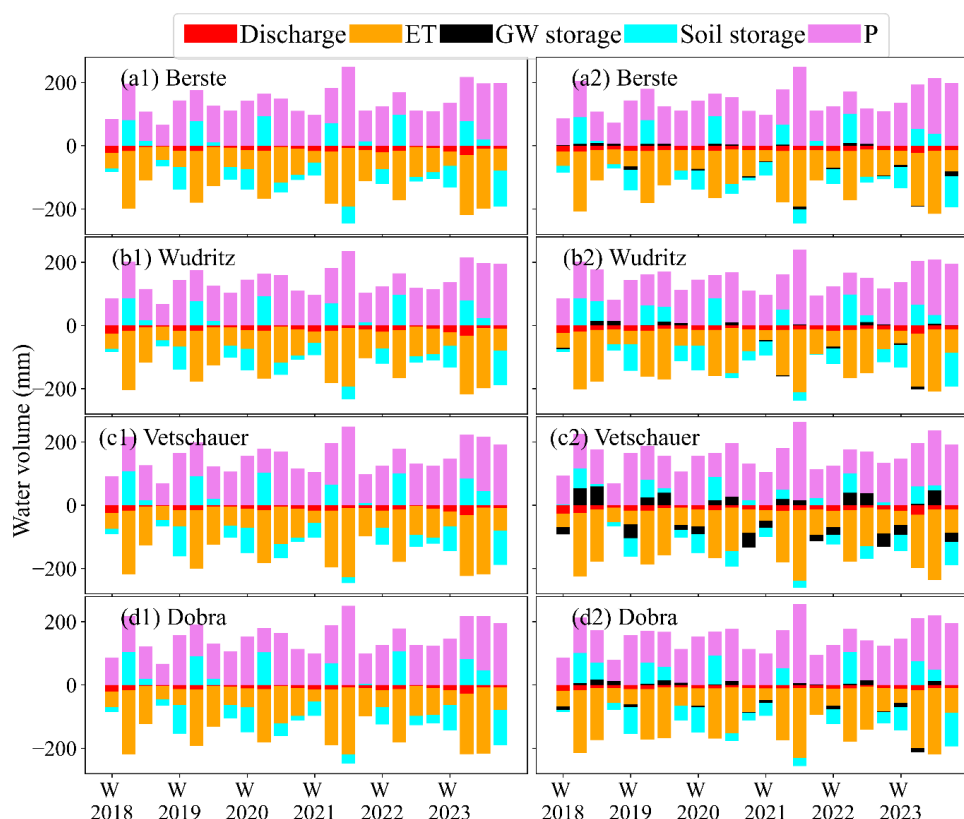
487

488 **3.3 Quantification of the water balance components**

489 The partitioning into different water balance components was relatively consistent across all
490 catchments, irrespective of the calibration schemes (Figure 8). ET was the dominant output
491 flux, especially during the spring and summer period (> 90%). Simulations showed that soil
492 storage played the major role in supplying water for ET in spring and early summer and was
493 subsequently replenished during autumn and winter. Discharge accounted for a minor
494 proportion of the water balance (~5%). Variations of groundwater storage in each season were
495 small (<1% of the total water balance) in simulations calibrated on discharge alone, while it



496 increased to ~5 - 30% (catchment dependent) when isotopes were included in calibrations
497 (Figure 8). With isotopes in calibrations, simulated groundwater storage declined during spring
498 and summer and was replenished in winter and fall, with the variation being the most
499 substantial in Vetschauer.



500

501 *Figure 8. Seasonal water balances in the four catchments. (a) Berste; (b) Wudritz; (c)*
502 *Vetschauer; (d) Dobra. Suffix “1” and “2” means averaged values of all simulations in the*
503 *Pareto front of scheme 1 and a compromised solution in schemes 2-5, respectively. Positive*
504 *bars represent water sources, while negative bars are water losses. “Channel storage” and*
505 *“Interception storage” were too small compared to other components to show in the figure.*



506 **4 Discussion**

507 **4.1 Model success for streamflow and isotope dynamics**

508 Streamflow usually serves as a key indicator of water resource availability and is widely used
509 in hydrological model calibration due to its broad accessibility. Previous work using isotopes
510 and other tracers has shown that calibration on streamflow alone can lead to misleading
511 conceptualization of hydrological processes (Ala-Aho et al., 2017; van Huijgevoort et al., 2016;
512 McDonnell and Beven 2014). However, similar to most studies based in environments where
513 blue water fluxes (i.e. streamflow and groundwater recharge) are greater than green water
514 fluxes (i.e. ET fluxes that sustain vegetation growth), here, streamflow dynamics and overall
515 runoff volumes were also effectively captured by discharge-only based calibrations in an ET-
516 dominated region. However, slight overestimations occurred during winter peaks and
517 underestimations during summer low-flow periods. In addition, modelled annual ET estimates
518 aligned closely with RS ET products (e.g., MODIS or PML), with ET amounts ~400 - 500
519 mm/year from dry (e.g., 2018) to wet (e.g., 2023) years and deviation of around ± 50 mm/year.
520 Although groundwater recharge was sometimes underestimated (especially in Berste), rough
521 partitioning of precipitation into green and blue water fluxes was accurately constrained by
522 streamflow in the calibrations. Similarly, in other literatures, multi-criteria calibrations
523 incorporating both streamflow and RS ET demonstrated marginal improvements in annual ET
524 or streamflow estimates, compared to discharge-only based calibrations, albeit with reduced
525 parameter equifinality (Oliveira et al., 2021; Shah et al., 2021).

526

527 However, discharge-only based calibrations normally exhibit significant uncertainty in
528 representing internal hydrological processes, owing to high degrees of model freedom and non-
529 identifiable parameters (Herrera et al., 2022). This was evidenced by the large uncertainty
530 bands in the simulated variables (for both streamflow and isotopes) under scheme 1. Moreover,



531 catchment discharge, as an output integrating upstream hydrological processes, provides only
532 limited insight into spatially distributed partitioning of water volumes and flow paths (Fatichi
533 et al., 2016). This limitation becomes more pronounced as models incorporate more complex
534 spatial disaggregation and physics-based process representations (Sun et al., 2017). A multi-
535 gauge regional streamflow calibration normally improves the spatial representativeness of
536 simulations and provides a greater constraint on relationships between catchment
537 characteristics and streamflow dynamics (Liu et al., 2020). However, internal mixing and
538 runoff generation processes (evidenced by isotope dynamics) under scheme 1 (which was a
539 multi-gauge streamflow calibration) did not show much difference to the single-gauge
540 calibrations (i.e., parameter set with best simulated streamflow in schemes 2-5). Improvements
541 on simulations of subsurface processes were also not clear in other literature (Wanders et al.,
542 2014). Furthermore, sensitivity analysis revealed that discharge was more sensitive to soil
543 drainage process in all three major land uses (i.e., forest, croplands, pasture) of the four studied
544 catchments, and parameters controlling other hydrological processes were less identifiable.

545

546 Incorporating stable water isotopes into modelling improves our understanding of
547 ecohydrological processes and storage dynamics. Multi-criteria calibration using both
548 streamflow and isotope enables exploration of a broader parameter space to satisfy multiple
549 calibration objectives (Holmes et al., 2020). Subsurface processes in the deeper layer (e.g.,
550 seepage and capillary flux in the present model) are inherently challenging to constrain in
551 modelling through only near-surface observations (e.g., ET, soil moisture), and these processes
552 are usually poorly understood (Beven, 2006). Stable water isotopes are powerful in this regard
553 as they integrate the cumulative effects of water flow paths and mixing across all hydrological
554 storages (Godsey et al. 2010). Our TAM revealed that discharge-only based calibration or
555 parameter sets with better simulated streamflow in isotope-aided calibrations does not



556 accurately capture such mixing processes, as their simulated isotopes are different from
557 observations. Model simulations that reconciled simulated and observed isotopes represented
558 better mixing between soil water and groundwater storage. Increased runoff from groundwater,
559 characterized by depleted isotopes, modulated modelled outflow signatures, flattening the
560 seasonal isotopic variability, and thus, increasing process representation. This aligns with
561 previous findings where dominant subsurface flows produce subtle isotopic variations
562 (Iorgulescu et al., 2007; Oerter and Bowen, 2019) and where contrasting isotope signatures
563 across water stores are key to disentangling water mixing processes (Kirchner, 2003).

564

565 The fractionation of stable water isotopes is governed by evaporation, and measured isotopes
566 at the catchment outlet reflected the aggregated evaporation rates across the whole catchment.
567 Parameters controlling ET processes (e.g., FC and LP) exhibited greater sensitivity when using
568 isotopes as a calibration target, supporting its value as a constraint on ET dynamics in
569 simulations. Despite this, total (bulk) seasonal ET volumes across the catchments showed
570 minimal variations along the Pareto front, implying that streamflow and isotopes similarly
571 constrain bulk ET estimates. The use of temporally quite coarse isotopic datasets – necessary
572 at such large spatial scale – and inter-annually averaged rainfall isotope inputs in this study
573 likely introduced uncertainty in ET process constraints, and higher-resolution data can better
574 capture temporal variability in fractionation intensity (Sprenger et al., 2017). This is consistent
575 with broader findings: while isotopic tracers are widely recognized for improving estimates of
576 E/T partitioning (Gibson and Edwards, 2002), their utility in refining total ET quantification
577 remains less clearly demonstrated, particularly at larger spatial scales.

578

579 **4.2 Water flux partitioning and influences of management measures**



580 Compared to simulations in the Berste, the ecohydrological partitioning was more reliably
581 represented in the Wudritz, Vetschauer and Dobra, as NSE or KGE of both streamflow and
582 isotopes reached > 0.4 in the compromised solutions (middle part of Pareto-optimal solutions).
583 In these catchments, runoff was predominantly generated from groundwater and soil storage,
584 reflecting a subsurface-process dominated flow regime. This pattern aligns with observations
585 across much of the Spree catchment, where subsurface-driven runoff mechanisms are
586 widespread (Chen et al., 2023). Runoff in the upper Spree catchment is predominantly
587 groundwater-driven (Kröcher et al., 2025), a pattern consistent with the Vetschauer catchment,
588 and likely shared by the Berste, as evidenced by depleted isotopic signatures. In contrast, the
589 Wudritz and Dobra catchments showed rather lower proportions of groundwater contributions.
590 This aligns with historically depressed groundwater levels caused by pumping during regional
591 de-watering from mining activities (Arndt and Heiland 2024). In addition, the influence of
592 groundwater in the studied four catchments may potentially increase, as the opencast mines
593 have been closed for 30 years and it is unclear to whether groundwater levels have fully
594 stabilized (Kröcher et al., 2025). The increased temperature and shift of precipitation from
595 summer to winter due to climate change also possibly leads to increased ET during winter and
596 spring reducing discharge and groundwater recharge accordingly. This could result in
597 contrasting water distributions in each season, and intensifying negative climatic water balance
598 in the local environment (Pohle et al., 2012).

599

600 In Wudritz and Dobra, isotope simulations optimized for streamflow accuracy produced more
601 isotopically depleted signatures compared to the measured values. To reconcile this
602 discrepancy, an assumption of lower proportions of transpiration in evapotranspiration (ET)
603 was needed. The mismatch in transpiration ratios between simulations and the PML product
604 may partially stem from unaccounted surface water evaporation. While evaporation from small



open water bodies (e.g., ponds, channels) has negligible impacts on overall the catchment water balance, it likely plays a critical role in isotopic enrichment (Birkel et al., 2011). For instance: in the Dobra (3.0% surface water area) and Wudritz (7.7% surface water area), isotopic concentrations were likely underestimated due to unmodeled surface water evaporation. The non-linear relationship between evaporation rate and isotopic enrichment, as described by the Craig-Gordon model (Craig and Gordon, 1965), explains this dynamic: early-stage evaporation induces stronger isotopic enrichment, approaching a threshold under constant environmental conditions (e.g., humidity, temperature). Thus, even relatively minor surface water evaporation can bias isotopic signatures which then impacts ET partitioning simulations.

In contrast, at Vetschauer (0.7% surface water area), the unaccounted surface water evaporation had minor effects on the modelling due to the minimal surface water area with simulations being more comparable to the PML estimates. The ability of stable water isotopes in constraining ET partitioning was also shown in the consistency between simulations and the PML estimates, which is similar to other applications (Birkel and Soulsby, 2015). Further, the small weight of isotopes in a scalar function combining multiple objectives meant that it was possible to disentangle ET processes (Wu et al., 2023). This was also illustrated by the minor adaptations in the Pareto front from better streamflow simulations to better isotope simulations. The transpiration ratios in the simulations along the Pareto front with better simulated isotopes at Vetschauer also aligned with the other sub-catchments of the Middle Spree (Landgraf et al., 2023). The normally contrasting transpiration ratios among different land uses (Schlesinger and Jasechko, 2014) were consistent with our simulations, and contrasting LAI in each land use explains these differences (Cao et al., 2022), although the PML estimation presented similar transpiration ratios among each land use. However, the transpiration ratios could be overestimated due to unparameterized irrigation effects (Paul-Limoges et al., 2022), and the



630 local water use efficiency should be further evaluated. The strong conflicts between using
631 streamflow or isotopes as calibration constraints resulted in incorrect representation of
632 transpiration ratios in Berste (0.3% surface water) along the Pareto front near the BSI. However,
633 simulations near the BSS still indicated a first approximation of transpiration, considering the
634 effectiveness of isotopes in differentiating ET partitioning.

635

636 Despite uncertainties introduced by multiple anthropogenic factors and influences, isotopes
637 were still valuable in ET partitioning in such heavily managed catchment. Since the Middle
638 Spree is an ET-dominated region and experiencing water scarcity due to replenishment of
639 historical groundwater withdrawn, evaluation of local water use efficiency in the croplands is
640 of great value for future water management. The preliminary assessment of ET partitioning
641 through isotope-aided modelling provides strong evidence in this aspect, although its trade-offs
642 with streamflow occasionally occurred due to unaccounted human impacts.

643

644 **4.3 Reasons for trade-offs between ecohydrological fluxes and future research directions**

645 Trade-offs in the calibrations between streamflow and isotopes are a common feature of TAM
646 (Holmes et al., 2020), though their severity varies across applications. The extent of these
647 compromises depends on the model's structural flexibility to assimilate additional constraints
648 (Holmes et al., 2020). Whilst some applications based on spatially-distributed models
649 presented slight conflicts in the information content of different calibration targets (Kuppel et
650 al., 2018), significant degradations in streamflow is found in a lumped model after
651 incorporating isotopes in calibration (Fenicia et al., 2008). In our study, the lack of explicit
652 information on anthropogenic drivers (e.g., water withdrawals, irrigations etc.) emerged as a
653 key contributor to trade-offs. Without parameterizing these factors, the model compensated by
654 adjusting flow velocities, which failed to replicate observed streamflow celerity during rainfall



655 events. The systematic biases were evidenced: parameter sets with better simulated streamflow
656 in isotope-aided calibrations produced a soil water-driven runoff regime and underestimated
657 baseflow, which were exacerbated by spring or summer water withdrawals altering natural
658 flow regimes. Measured isotopic damping (flattened variations) implied slower flow velocities
659 and greater groundwater contributions, yet the model was unable to capture these processes
660 from streamflow dynamics alone. The strongest trade-offs occurred in the Berste catchment,
661 where extensive croplands and likely high irrigation withdrawals amplified mismatches
662 between simulated and observed hydrological behavior.

663

664 These trade-offs could be partially mitigated by integrating more process-based
665 conceptualizations, though this often requires more complex parameterizations. While such
666 enhancements improve a model's ability to simultaneously adapt flow velocity and celerity,
667 they also introduce greater simulation uncertainty (Herrera et al., 2022). Simple explicit
668 modeling of water extraction for irrigation (e.g., channel-to-cropland transfers) could alleviate
669 trade-offs observed in this study. However, sparse records of withdrawal volumes and
670 irrigation patterns, as well as political sensitivities in data sharing may limit practical modelling.
671 The STARR model's simplified routing structure, where runoff from contrasting sources
672 follows identical pathways to the outlet, diverges from more physics-based frameworks that
673 better spatially differentiate the timing of contributions of overland flow, unsaturated zone flow,
674 and groundwater flow. While this conceptual routing captured flow celerity by adjusting
675 discharge coefficients (i.e., k_S , k_G), it systematically overestimated flow velocity, creating
676 conflicts in multi-criteria calibrations (McDonnell and Beven 2014).

677

678 Conventional calibration metrics like NSE or KGE could hamper the exploration of accurate
679 catchment processes, as single statistical performance measures are unable to capture all



680 features of observed variables (Gupta et al., 1998). Seasonal isotope observations increased
681 bias sensitivity and skewed performance assessments under the present metrics. Metrics
682 underscoring seasonal variability could be more indicative on runoff generation processes. In
683 order to capture observations at different temporal scales, wavelet-based objectives could be
684 alternative in this context (Manikanta and Vema, 2022). In addition, anthropogenic activities
685 (e.g., water withdrawn mainly occurred during spring and summer) were intensively
686 implemented in specific seasons and not in others. Using metrics which weaken the influences
687 of these epistemic errors in the observed streamflow could be a potential way to derive more
688 correct parameter sets. In this regard, the limits-of-acceptability method, defining lower and
689 upper boundaries as the tolerance of simulations deviations, is potentially useful in such heavily
690 managed catchments (Beven, 2006), although setting the limits is still challenging due to the
691 lack of specific information of many management interventions (Wu et al., 2025).

692

693 Despite having limited streamwater isotope samples due to the large scale of the sampled area,
694 they were sufficient and actually very valuable to reveal some significant difference between
695 catchments. This helped to better understand ecohydrological processes and to identify
696 processes that were not adequately captured, such as some of the anthropogenic impacts
697 discussed above. Isotope data at finer temporal resolution could help to better constrain ET
698 partitioning processes in heavily modified catchments, as they certainly do in more natural
699 environments (Soulsby et al., 2015). In addition, precipitation isotopes were from a global data
700 product (Bowen and Revenaugh, 2003). The use of interannually averaged monthly values
701 likely failed to capture short-term climate variability or anthropogenic influences (e.g., fossil
702 fuel-derived vapor), introducing errors in water source apportionment (e.g., hydrograph
703 separation) (Xia et al., 2024; Yang and Yoshimura, 2024). Again, high resolution local data
704 would be advantageous for such investigations.



705 **5 Conclusions**

706 Stable water isotopes are valuable tracers in tracking hydrological flow paths and identifying
707 water sources, offering the potential to constrain equifinality in ecohydrological models. While
708 model calibration in natural catchments typically exhibits slight trade-offs between isotopic
709 signatures and conventional hydrological variables (e.g., discharge), this study advances a
710 novel perspective on the benefits and challenges of integrating isotopes in heavily human-
711 impacted catchments. Using the conceptual-based, fully-distributed TAM STARR, we
712 calibrated both isotopes and streamflow without explicitly parameterizing anthropogenic
713 disturbances to investigate three critical issues: (1) the influence of human interventions on
714 model performance, (2) the potential of using discharge alone in calibration to mislead process
715 interrelations from simulations under anthropogenic stress, and (3) the adaptability and value
716 of isotopes in such contexts. We studied four sub-catchments of the Middle Spree (Berste,
717 Wudritz, Vetschauer, and Dobra), subjected to contrasting anthropogenic pressures (long-term
718 mining impacts, seasonal water withdrawals), and derived Pareto-optimal solutions to
719 disentangle the additional insights provided by isotope-aided calibration compared with
720 streamflow alone.

721 The results demonstrate that strong trade-offs between isotopes and streamflow in calibrations
722 arise in such anthropogenically-impacted catchments, where unquantified epistemic errors in
723 streamflow observations caused by human activities compromise model reliability. Notably,
724 discharge-only based calibrations could mis-represent runoff partitioning processes, especially
725 in catchments with water withdrawals for irrigation, while isotopes helped identify implausible
726 simulations by more realistic process representation. The four study catchments were ET
727 dominated, and groundwater contributions to runoff were site specific. For example,
728 Vetschauer displayed the most dynamic vertical fluxes, with groundwater storage fluctuations
729 similar to soil storage in magnitude in the water balance, while Wudritz and Dobra showed



730 minor groundwater contributions, consistent with the long-term mining effects. Isotope
731 fractionation was very sensitive to the proportion of surface water area, and the absence of
732 parameterising intermittent restored mining lakes in catchments resulted in worse results in ET
733 partitioning processes. Further, isotopes help to disentangle ET partitioning, even if strong
734 trade-offs in calibrations between streamflow and isotopes occurred.

735 This study highlights how unaccounted anthropogenic activities can alter model interpretations
736 and underscores the complementary role of isotopes and TAMs in refining simulations under
737 complex human-environment interactions, although only seasonally sampled isotopes were
738 employed. While distinct trade-offs between streamflow and isotopes were observed in the
739 study catchments, with Pareto-optimal solutions (e.g., Berste) failing to meet acceptable
740 performance thresholds, these simulations still offer informative insights into ecohydrological
741 dynamics and partitioning in heavily impacted catchments, even when quantitative process
742 evaluation remains challenging. In catchments subject to intensive anthropogenic interventions
743 (e.g., altered water distribution via irrigation or withdrawals), the severity of streamflow-
744 isotope conflicts and compromises in TAM may serve as an indirect diagnostic of human
745 impacts on water partitioning. Representing anthropogenic effects in ecohydrological models
746 is inherently difficult, particularly when historical data on water use or management practices
747 are sparse. However, we demonstrated here that TAMs are still very valuable in such
748 applications.

749

750 **Acknowledgement**

751 Hanwu Zheng is funded by the Chinese Scholarship Council (CSC). Tetzlaff's contribution was partly funded
752 through the Einstein Research Unit "Climate and Water under Change" from the Einstein Foundation Berlin and
753 Berlin University Alliance (grant no. ERU-2020- 609) and through the WETSCAPES2.0 project (DFG TRR410/1
754 2025). Birkel's contribution was supported by a senior research fellowship of IGB and a sabbatical license by



- 755 UCR. Contributions from Soulsby were supported by the Leibnitz Association Germany in the project Wetland
756 Restoration in Peatlands and Mosaic II funded by Einstein Foundation.



757 **Reference:**

- 758 Ala-Aho, P., Tetzlaff, D., McNamara, J.P., Laudon, H., Soulsby, C., 2017. Using isotopes to
759 constrain water flux and age estimates in snow-influenced catchments using the STARR
760 (Spatially distributed Tracer-Aided Rainfall-Runoff) model. *Hydrol. Earth Syst. Sci.* 21,
761 5089–5110. <https://doi.org/10.5194/hess-21-5089-2017>
- 762 Arndt, S., Heiland, S., 2024. Current status of water-related planning for climate change
763 adaptation in the Spree River basin, Germany. <https://doi.org/10.5194/nhess-2024-59>
- 764 Beven, K., 2006. A manifesto for the equifinality thesis. *J. Hydrol.* 320, 18–36.
765 <https://doi.org/10.1016/j.jhydrol.2005.07.007>
- 766 Birkel, C., Soulsby, C., 2015. Advancing tracer-aided rainfall-runoff modelling: A review of
767 progress, problems and unrealised potential. *Hydrol. Process.* 29, 5227–5240.
768 <https://doi.org/10.1002/hyp.10594>
- 769 Birkel, C., Soulsby, C., Tetzlaff, D., 2011. Modelling catchment-scale water storage dynamics:
770 Reconciling dynamic storage with tracer-inferred passive storage. *Hydrol. Process.* 25,
771 3924–3936. <https://doi.org/10.1002/hyp.8201>
- 772 Blank, J., Deb, K., 2020. Pymoo: Multi-Objective Optimization in Python. *IEEE Access* 8,
773 89497–89509. <https://doi.org/10.1109/ACCESS.2020.2990567>
- 774 Bowen, G.J., Revenaugh, J., 2003. Interpolating the isotopic composition of modern meteoric
775 precipitation. *Water Resour. Res.* 39, 1–13. <https://doi.org/10.1029/2003WR002086>
- 776 Cao, R., Huang, H., Wu, G., Han, D., Jiang, Z., Di, K., Hu, Z., 2022. Spatiotemporal variations
777 in the ratio of transpiration to evapotranspiration and its controlling factors across
778 terrestrial biomes. *Agric. For. Meteorol.* 321, 108984.
779 <https://doi.org/10.1016/j.agrformet.2022.108984>
- 780 Chakraborty, S., Belekar, A.R., Datye, A., Sinha, N., 2018. Isotopic study of intraseasonal
781 variations of plant transpiration: An alternative means to characterise the dry phases of



- monsoon. *Sci. Rep.* 8, 1–11. <https://doi.org/10.1038/s41598-018-26965-6>
- Chen, K., Tetzlaff, D., Goldhammer, T., Freymueller, J., Wu, S., Andrew Smith, A., Schmidt, A., Liu, G., Venohr, M., Soulsby, C., 2023. Synoptic water isotope surveys to understand the hydrology of large intensively managed catchments. *J. Hydrol.* 623, 129817. <https://doi.org/10.1016/j.jhydrol.2023.129817>
- Chow, V. Te, 1959. *Open-channel hydraulics*, Erlangga : Bandung. McGraw-Hill civil engineering series Civil.
- Correa, A., Birkel, C., Gutierrez, J., Dehaspe, J., Durán-Quesada, A.M., Soulsby, C., Sánchez-Murillo, R., 2020. Modelling non-stationary water ages in a tropical rainforest: A preliminary spatially distributed assessment. *Hydrol. Process.* 34, 4776–4793. <https://doi.org/10.1002/hyp.13925>
- Craig, H., Gordon, L.I., 1965. Isotopic oceanography: deuterium and oxygen-18 variation in the ocean and the marine atmosphere, in: *Stable Isotopes in Oceanographic Studies and Paleotemperatures*. Laboratorio di Geologia Nucleare, Pisa.
- Deb, K., Pratap, A., Agarwal, S., Meyarivan, T., 2002. A fast and elitist multiobjective genetic algorithm: NSGA-II. *IEEE Trans. Evol. Comput.* 6, 182–197. <https://doi.org/10.1109/4235.996017>
- Dehaspe, J., Birkel, C., Tetzlaff, D., Sánchez-Murillo, R., Durán-Quesada, A.M., Soulsby, C., 2018. Spatially distributed tracer-aided modelling to explore water and isotope transport, storage and mixing in a pristine, humid tropical catchment. *Hydrol. Process.* 32, 3206–3224. <https://doi.org/10.1002/hyp.13258>
- Deutscher Wetterdienst (DWD), 2024. Daily station observations (temperature, pressure, precipitation, sunshine duration, etc.) for Germany. URL <https://cdc.dwd.de/portal/> (accessed 5.25.24).
- Efstratiadis, A., Koutsoyiannis, D., 2010. One decade of multi-objective calibration approaches



- 807 in hydrological modelling : a review 6667. <https://doi.org/10.1080/02626660903526292>
- 808 Fatichi, S., Vivoni, E.R., Ogden, F.L., Ivanov, V.Y., Mirus, B., Gochis, D., Downer, C.W.,
- 809 Camporese, M., Davison, J.H., Ebel, B., Jones, N., Kim, J., Mascaro, G., Niswonger, R.,
- 810 Restrepo, P., Rigon, R., Shen, C., Sulis, M., Tarboton, D., 2016. An overview of current
- 811 applications, challenges, and future trends in distributed process-based models in
- 812 hydrology. *J. Hydrol.* 537, 45–60. <https://doi.org/10.1016/j.jhydrol.2016.03.026>
- 813 Fenicia, F., McDonnell, J.J., Savenije, H.H.G., 2008. Learning from model improvement: On
- 814 the contribution of complementary data to process understanding. *Water Resour. Res.* 44,
- 815 1–13. <https://doi.org/10.1029/2007WR006386>
- 816 Gibson, J.J., Edwards, T.W.D., 2002. Regional water balance trends and evaporation-
- 817 transpiration partitioning from a stable isotope survey of lakes in northern Canada. *Global*
- 818 *Biogeochem. Cycles* 16, 10-1-10–14. <https://doi.org/10.1029/2001gb001839>
- 819 Godsey, S. E., W. Aas, T. A. Clair, et al. 2010. “Generality of Fractal 1/f Scaling in Catchment
- 820 Tracer Time Series, and Its Implications for Catchment Travel Time Distributions.”
- 821 *Hydrological Processes* 24, no. 12: 1660–1671. <https://doi.org/10.1002/hyp.7677>.
- 822 Guevara-Escobar, A., Gonzalez-Sosa, E., Ramos-Salinas, M., Hernandez-Delgado, G.D., 2007.
- 823 Experimental analysis of drainage and water storage of litter layers. *Hydrol. Earth Syst.*
- 824 *Sci.* 11, 1703–1716. <https://doi.org/10.5194/hess-11-1703-2007>
- 825 Gupta, H.V., Sorooshian, S., Yapo, P.O., 1998. Toward improved calibration of hydrologic
- 826 models: Multiple and noncommensurable measures of information. *Water Resour. Res.*
- 827 34, 751–763. <https://doi.org/10.1029/97WR03495>
- 828 Herrera, P.A., Marazuela, M.A., Hofmann, T., 2022. Parameter estimation and uncertainty
- 829 analysis in hydrological modeling. *Wiley Interdiscip. Rev. Water* 9, 1–23.
- 830 <https://doi.org/10.1002/wat2.1569>
- 831 Hodson, T.O., 2022. Root-mean-square error (RMSE) or mean absolute error (MAE): when to



- 832 use them or not. *Geosci. Model Dev.* 15, 5481–5487. <https://doi.org/10.5194/gmd-15->
833 5481-2022
- 834 Holmes, T., Stadnyk, T.A., Kim, S.J., Asadzadeh, M., 2020. Regional Calibration With Isotope
835 Tracers Using a Spatially Distributed Model : A Comparison of Methods. *Water Resour.*
836 *Res.* 56. <https://doi.org/10.1029/2020WR027447>
- 837 Hrachowitz, M., Savenije, H.H.G., Blöschl, G., McDonnell, J.J., Sivapalan, M., Pomeroy, J.W.,
838 Arheimer, B., Blume, T., Clark, M.P., Ehret, U., Fenicia, F., Freer, J.E., Gelfan, A., Gupta,
839 H. V., Hughes, D.A., Hut, R.W., Montanari, A., Pande, S., Tetzlaff, D., Troch, P.A.,
840 Uhlenbrook, S., Wagener, T., Winsemius, H.C., Woods, R.A., Zehe, E., Cudennec, C.,
841 2013. A decade of Predictions in Ungauged Basins (PUB)-a review. *Hydrol. Sci. J.* 58,
842 1198–1255. <https://doi.org/10.1080/02626667.2013.803183>
- 843 Iorgulescu, I., Beven, K.J., Musy, A., 2007. Flow, mixing, and displacement in using a data-
844 based hydrochemical model to predict conservative tracer data. *Water Resour. Res.* 43, 1–
845 12. <https://doi.org/10.1029/2005WR004019>
- 846 Jung, H., Tetzlaff, D., Birkel, C., Soulsby, C., 2025. Recent Developments and Emerging
847 Challenges in Tracer-Aided Modeling. *WIREs Water* 12.
848 <https://doi.org/10.1002/wat2.70015>
- 849 Karssenbergh, D., Schmitz, O., Salamon, P., de Jong, K., Bierkens, M.F.P., 2010. A software
850 framework for construction of process-based stochastic spatio-temporal models and data
851 assimilation. *Environ. Model. Softw.* 25, 489–502.
852 <https://doi.org/10.1016/j.envsoft.2009.10.004>
- 853 Kirchner, J.W., 2006. Getting the right answers for the right reasons: Linking measurements,
854 analyses, and models to advance the science of hydrology. *Water Resour. Res.* 42, 1–5.
855 <https://doi.org/10.1029/2005WR004362>
- 856 Kirchner, J.W., 2003. A double paradox in catchment hydrology and geochemistry. *Hydrol.*



- 857 Process. 17, 871–874. <https://doi.org/10.1002/hyp.5108>
- 858 Klaus, J., McDonnell, J.J., 2013. Hydrograph separation using stable isotopes: Review and
859 evaluation. *J. Hydrol.* 505, 47–64. <https://doi.org/10.1016/j.jhydrol.2013.09.006>
- 860 Kröcher, J., Ghazaryan, G., Lischeid, G., 2025. Unravelling Regional Water Balance Dynamics
861 in Anthropogenically Shaped Lowlands: A Data-Driven Approach. *Hydrol. Process.* 39,
862 1–17. <https://doi.org/10.1002/hyp.70053>
- 863 Kuppel, S., Tetzlaff, D., Maneta, M.P., Soulsby, C., 2018. What can we learn from multi-data
864 calibration of a process-based ecohydrological model? *Environ. Model. Softw.* 101, 301–
865 316. <https://doi.org/10.1016/j.envsoft.2018.01.001>
- 866 Landesregierung Brandenburg, 2024. Landesamt für Umwelt Brandenburg (LfU). URL
867 <https://lfu.brandenburg.de/lfu/de/> (accessed 5.25.24).
- 868 Landgraf, J., Tetzlaff, D., Birkel, C., Stevenson, J.L., Soulsby, C., 2023. Assessing land use
869 effects on ecohydrological partitioning in the critical zone through isotope-aided
870 modelling. *Earth Surf. Process. Landforms* 48, 3199–3219.
871 <https://doi.org/10.1002/esp.5691>
- 872 Lindström, G., Johansson, B., Persson, M., Gardelin, M., Bergström, S., 1997. Development
873 and test of the distributed HBV-96 hydrological model. *J. Hydrol.* 201, 272–288.
874 [https://doi.org/10.1016/S0022-1694\(97\)00041-3](https://doi.org/10.1016/S0022-1694(97)00041-3)
- 875 Liu, J., Liu, X., Wang, Y., Li, Y., Jiang, Y., Fu, Y., Wu, Y.J.Á.Y.F.Á.J., 2020. Landscape
876 composition or configuration : which contributes more to catchment hydrological flows
877 and variations ? *Landsc. Ecol.* 35, 1531–1551. [https://doi.org/10.1007/s10980-020-](https://doi.org/10.1007/s10980-020-01035-3)
878 01035-3
- 879 Luo, S., Tetzlaff, D., Smith, A., Soulsby, C., 2024. Assessing impacts of alternative land use
880 strategies on water partitioning, storage and ages in drought-sensitive lowland catchments
881 using tracer-aided ecohydrological modelling. *Hydrol. Process.* 38, 1–21.



- 882 <https://doi.org/10.1002/hyp.15126>
- 883 Manikanta, V., Vema, V.K., 2022. Formulation of Wavelet Based Multi-Scale Multi-Objective
- 884 Performance Evaluation (WMMPE) Metric for Improved Calibration of Hydrological
- 885 Models. *Water Resour. Res.* 58, 1–20. <https://doi.org/10.1029/2020WR029355>
- 886 Marx, C., Tetzlaff, D., Hinkelmann, R., Soulsby, C., 2021. Isotope hydrology and water
- 887 sources in a heavily urbanized stream. *Hydrol. Process.* 35, 1–20.
- 888 <https://doi.org/10.1002/hyp.14377>
- 889 McDonnell, J.J., Beven, K., 2014. Debates - The future of hydrological sciences: A (common)
- 890 path forward? A call to action aimed at understanding velocities, celerities and residence
- 891 time distributions of the headwater hydrograph. *Water Resour. Res.* 50, 5342–5350.
- 892 <https://doi.org/10.1002/2013WR015141>
- 893 McDonnell, J.J., Sivapalan, M., Vaché, K., Dunn, S., Grant, G., Haggerty, R., Hinz, C., Hooper,
- 894 R., Kirchner, J., Roderick, M.L., Selker, J., Weiler, M., 2007. Moving beyond
- 895 heterogeneity and process complexity: A new vision for watershed hydrology. *Water*
- 896 *Resour. Res.* 43, 1–6. <https://doi.org/10.1029/2006WR005467>
- 897 Morris, M.D., 1991. Factorial sampling plans for preliminary computational experiments.
- 898 *Technometrics* 33, 161–174.
- 899 Oerter, E.J., Bowen, G.J., 2019. Spatio-temporal heterogeneity in soil water stable isotopic
- 900 composition and its ecohydrologic implications in semiarid ecosystems. *Hydrol. Process.*
- 901 33, 1724–1738. <https://doi.org/10.1002/hyp.13434>
- 902 Oliveira, A.M., Fleischmann, A.S., Paiva, R.C.D., 2021a. On the contribution of remote
- 903 sensing-based calibration to model hydrological and hydraulic processes in tropical
- 904 regions. *J. Hydrol.* 597, 126184. <https://doi.org/10.1016/j.jhydrol.2021.126184>
- 905 Paul-Limoges, E., Revill, A., Maier, R., Buchmann, N., Damm, A., 2022. Insights for the
- 906 Partitioning of Ecosystem Evaporation and Transpiration in Short-Statured Croplands. *J.*



- 907 Geophys. Res. Biogeosciences 127, 1–19. <https://doi.org/10.1029/2021JG006760>
- 908 Pianosi, F., Sarrazin, F., Wagener, T., 2015. A Matlab toolbox for Global Sensitivity Analysis.
- 909 Environ. Model. Softw. 70, 80–85. <https://doi.org/10.1016/j.envsoft.2015.04.009>
- 910 Pohle, I., Koch, H., Grünewald, U., 2012. Potential climate change impacts on the water
- 911 balance of subcatchments of the River Spree, Germany. Adv. Geosci. 32, 49–53.
- 912 <https://doi.org/10.5194/adgeo-32-49-2012>
- 913 Pusch, M., Andersen, H.E., Behrendt, H., Tor, M., Hoffmann, C.C., Kronvang, B., Pedersen,
- 914 M.L., Tor, M., Wolter, C., 2009. Rivers of the Central European Highlands and Plains
- 915 525–576. <https://doi.org/10.1016/B978-0-12-369449-2.00014-X>
- 916 Pusch, M., Hoffmann, A., 2000. Conservation concept for a river ecosystem (River Spree,
- 917 Germany) impacted by flow abstraction in a large post-mining area. Landsc. Urban Plan.
- 918 51, 165–176. [https://doi.org/10.1016/S0169-2046\(00\)00107-9](https://doi.org/10.1016/S0169-2046(00)00107-9)
- 919 Rutter, A.J., Kershaw, K.A., Robins, P.C., Morton, A.J., 1972. A predictive Model of Rainfall
- 920 Interception in Forests. Agric. Meteorol. 9, 367–384.
- 921 Schlesinger, W.H., Jasechko, S., 2014. Transpiration in the global water cycle. Agric. For.
- 922 Meteorol. 189–190, 115–117. <https://doi.org/10.1016/j.agrformet.2014.01.011>
- 923 Scudeler, C., Pangle, L., Pasetto, D., Niu, G.Y., Volkmann, T., Paniconi, C., Putti, M., Troch,
- 924 P., 2016. Multiresponse modeling of variably saturated flow and isotope tracer transport
- 925 for a hillslope experiment at the Landscape Evolution Observatory. Hydrol. Earth Syst.
- 926 Sci. 20, 4061–4078. <https://doi.org/10.5194/hess-20-4061-2016>
- 927 Seibert, J., Vis, M.J.P., 2012. Teaching hydrological modeling with a user-friendly catchment-
- 928 runoff-model software package. Hydrol. Earth Syst. Sci. 16, 3315–3325.
- 929 <https://doi.org/10.5194/hess-16-3315-2012>
- 930 Shah, S., Duan, Z., Song, X., Li, R., Mao, H., Liu, J., Ma, T., Wang, M., 2021. Evaluating the
- 931 added value of multi-variable calibration of SWAT with remotely sensed



- 932 evapotranspiration data for improving hydrological modeling. *J. Hydrol.* 603, 127046.
933 <https://doi.org/10.1016/j.jhydrol.2021.127046>
- 934 Shen, H., Tolson, B.A., Mai, J., 2022. Time to Update the Split-Sample Approach in
935 Hydrological Model Calibration. *Water Resour. Res.* 58, 1–26.
936 <https://doi.org/10.1029/2021WR031523>
- 937 Simůnek, J., Sejna, M., Saito, H., van Genuchten, M.T., 2013. The HYDRUS-1D Software
938 Package for Simulating the One-Dimensional Movement of Water, Heat, and Multiple
939 Solutes in Variably-Saturated Media. *Dep. Environ. Sci. Calif. RIVERSIDERIVERSIDE*,
940 Calif.
- 941 Smith, A., Tetzlaff, D., Kleine, L., Maneta, M., Soulsby, C., 2021. Quantifying the effects of
942 land use and model scale on water partitioning and water ages using tracer-aided
943 ecohydrological models. *Hydrol. Earth Syst. Sci.* 25, 2239–2259.
944 <https://doi.org/10.5194/hess-25-2239-2021>
- 945 Smith, A.A., Tetzlaff, D., Maneta, M., Soulsby, C., 2022. Critical Zone Response Times and
946 Water Age Relationships Under Variable Catchment Wetness States: Insights Using a
947 Tracer-Aided Ecohydrological Model. *Water Resour. Res.* 58.
948 <https://doi.org/10.1029/2021WR030584>
- 949 Soulsby, C., Birkel, C., Geris, J., Dick, J., Tunaley, C., Tetzlaff, D., 2015. Stream water age
950 distributions controlled by storage dynamics and nonlinear hydrologic connectivity:
951 Modeling with high-resolution isotope data. *Water Resour. Res.* 51, 7759–7776.
952 <https://doi.org/10.1002/2015WR017888>
- 953 Sprenger, M., Tetzlaff, D., Soulsby, C., 2017. Soil water stable isotopes reveal evaporation
954 dynamics at the soil-plant-atmosphere interface of the critical zone. *Hydrol. Earth Syst.*
955 *Sci.* 21, 3839–3856. <https://doi.org/10.5194/hess-21-3839-2017>
- 956 Sprenger, M., Volkmann, T.H.M., Blume, T., Weiler, M., 2015. Estimating flow and transport



- 957 parameters in the unsaturated zone 2617–2635. <https://doi.org/10.5194/hess-19-2617->
958 2015
- 959 Stevenson, J.L., Birkel, C., Comte, J.C., Tetzlaff, D., Marx, C., Neill, A., Maneta, M., Boll, J.,
960 Soulsby, C., 2023. Quantifying heterogeneity in ecohydrological partitioning in urban
961 green spaces through the integration of empirical and modelling approaches. *Environ.*
962 *Monit. Assess.* 195. <https://doi.org/10.1007/s10661-023-11055-6>
- 963 Sun, W., Wang, Y., Wang, G., Cui, X., Yu, J., Zuo, D., Xu, Z., 2017. Physically based
964 distributed hydrological model calibration based on a short period of streamflow data:
965 case studies in four Chinese basins. *Hydrol. Earth Syst. Sci.* 21, 251–265.
966 <https://doi.org/10.5194/hess-21-251-2017>
- 967 van der Sande, C.J., de Jong, S.M., de Roo, A.P.J., 2003. A segmentation and classification
968 approach of IKONOS-2 imagery for land cover mapping to assist flood risk and flood
969 damage assessment. *Int. J. Appl. Earth Obs. Geoinf.* 4, 217–229.
970 [https://doi.org/10.1016/S0303-2434\(03\)00003-5](https://doi.org/10.1016/S0303-2434(03)00003-5)
- 971 van Huijgevoort, M.H.J., Tetzlaff, D., Sutanudjaja, E.H., Soulsby, C., 2016. Using high
972 resolution tracer data to constrain water storage, flux and age estimates in a spatially
973 distributed rainfall-runoff model. *Hydrol. Process.* 30, 4761–4778.
974 <https://doi.org/10.1002/hyp.10902>
- 975 Von Hoyningen-Huene, J., 1981. Die Interzeption des Niederschlages in landwirtschaftlichen
976 Pflanzenbeständen. *Arbeitsbericht Deutscher Verband fuer Wasserwirtschaft und*
977 *Kulturbau, Schriftenr. dtsh. verb. wasserwirtsch. kulturbau, hamburg berlin. DVWK,*
978 *Braunschweig, Germany.* https://doi.org/10.1007/978-3-642-41714-6_91316
- 979 Wada, Y., Bierkens, M.F.P., De Roo, A., Dirmeyer, P.A., Famiglietti, J.S., Hanasaki, N., Konar,
980 M., Liu, J., Schmied, H.M., Oki, T., Pokhrel, Y., Sivapalan, M., Troy, T.J., Van Dijk,
981 A.I.J.M., Van Emmerik, T., Van Huijgevoort, M.H.J., Van Lanen, H.A.J., Vörösmarty,



- 982 C.J., Wanders, N., Wheatler, H., 2017. Human-water interface in hydrological modelling:
983 Current status and future directions. *Hydrol. Earth Syst. Sci.* 21, 4169–4193.
984 <https://doi.org/10.5194/hess-21-4169-2017>
- 985 Wanders, N., Bierkens, M.F.P., de Jong, S.M., de Roo, A., Karssenbergh, D., 2014. The benefits
986 of using remotely sensed soil moisture in parameter identification of large-scale
987 hydrological models. *Water Resour. Res.* 50, 6874–6891.
988 <https://doi.org/10.1002/2013WR014639>
- 989 Wu, S., Tetzlaff, D., Beven, K., Soulsby, C., 2025. DREAM(LoAX): Simultaneous Calibration
990 and Diagnosis for Tracer-Aided Ecohydrological Models Under the Equifinality Thesis.
991 *Water Resour. Res.* 61. <https://doi.org/10.1029/2024WR038779>
- 992 Wu, S., Tetzlaff, D., Yang, X., Smith, A., Soulsby, C., 2023. Integrating Tracers and Soft Data
993 Into Multi-Criteria Calibration: Implications From Distributed Modeling in a Riparian
994 Wetland. *Water Resour. Res.* 59, 1–21. <https://doi.org/10.1029/2023WR035509>
- 995 Xia, C., Zuecco, G., Marchina, C., Penna, D., Borga, M., 2024. Effects of Short-Term Climate
996 Variations on Young Water Fraction in a Small Pre-Alpine Catchment. *Water Resour.*
997 *Res.* 60, 1–22. <https://doi.org/10.1029/2023WR036245>
- 998 Yang, X., Tetzlaff, D., Müller, C., Knöller, K., Borchardt, D., Soulsby, C., 2023. Upscaling
999 Tracer-Aided Ecohydrological Modeling to Larger Catchments: Implications for Process
1000 Representation and Heterogeneity in Landscape Organization. *Water Resour. Res.* 59.
1001 <https://doi.org/10.1029/2022WR033033>
- 1002 Yang, Y., Yoshimura, K., 2024. Simulation of Water Isotopes in Combustion-Derived Vapor
1003 Emissions in Winter. *J. Geophys. Res. Atmos.* 129.
1004 <https://doi.org/10.1029/2023JD040543>
- 1005 Zhang, Y., Kong, D., Gan, R., Chiew, F.H.S., McVicar, T.R., Zhang, Q., Yang, Y., 2019.
1006 Coupled estimation of 500 m and 8-day resolution global evapotranspiration and gross



1007 primary production in 2002–2017. Remote Sens. Environ. 222, 165–182.

1008 <https://doi.org/10.1016/j.rse.2018.12.031>

1009

1010

1011

1012